PAPER

Check for updates

Magnetic behaviour of a spin-canted asymmetric lanthanide quinolate trimer†

Lester Batista, [ID] [a] Sagar Paul, [ID] [b] Concepción Molina-Jirón, [ID] *[c,d]
Juan A. Jaén, [ID] [e,f] Dieter Fensker, [g] Olaf Fuhr, [ID] [g,h] Mario Ruben, [ID] *[d,g,i]
Wolfgang Wernsdorfer [ID] *[b,d] and Eufemio Moreno-Pineda [ID] *[b,e,f]

An asymmetrical dysprosium trimer with a molecular formula of **[Dy₃(hq)₇(hqH)(NO₃)₂(H₂O)]** was obtained through a reflux reaction employing as starting material $Dy(NO_3)_3 \cdot nH_2O$ and 8-quinolinoline as ligand. Magnetic susceptibility investigations show the system to be an SMM, which was corroborated by sub-Kelvin μSQUID studies. Upon cooling, the magnetic susceptibility also exhibits a decrease in the $\chi_M T$ product, which was confirmed to be due to intramolecular antiferromagnetic interactions. μSQUID measurements, moreover, reveal a marked magnetic behaviour in the angular dependence of the hysteresis loops. The latter is a direct consequence of the non-colinear spin arrangement of the anisotropy axes of each Dy(III) ion in **[Dy₃(hq)₇(hqH)(NO₃)₂(H₂O)]** and the interaction between the ions, as also evidenced by CASSCF calculations. Our results evidence the effect of spin canting along with the intramolecular interactions, which can induce non-trivial magnetic behaviour in SMMs.

Introduction

The fascinating phenomenon of slow magnetic relaxation in molecular systems was first observed for the transition metal aggregate $[Mn_{12}O_{12}(OAc)_{16}(H_2O)_4]\cdot 4H_2O \cdot 2AcOH$ best known as $\{Mn_{12}\}$[1,2] and years later in a lanthanide-based molecule with formula $[LnPc_2]^- \cdot TBA^+$ (TBA^+ = tetrabutylammonium) where

ᵃUniversidad de Panamá, Facultad de Ciencias Naturales, Exactas y Tecnología, Depto. Física, 0824, Panamá

ᵇPhysikalisches Institut, Karlsruhe Institute of Technology, D-76131 Karlsruhe, Germany. E-mail: wolfgang.wernsdorfer@kit.edu

ᶜUniversidad de Panamá, Facultad de Ciencias Naturales, Exactas y Tecnología, Depto. de Bioquímica, 0824, Panamá. E-mail: concepcion.molina@up.ac.pa

ᵈInstitute of Quantum Materials and Technologies (IQMT), Karlsruhe Institute of Technology (KIT), Hermann-von-Helmholtz-Platz 1, 76344 Eggenstein-Leopoldshafen, Germany. E-mail: mario.ruben@kit.edu

ᵉUniversidad de Panamá, Facultad de Ciencias Naturales, Exactas y Tecnología, Depto. de Química-Física, 0824, Panamá. E-mail: eufemio.moreno@up.ac.pa

ᶠUniversidad de Panamá, Facultad de Ciencias Naturales, Exactas y Tecnología, Grupo de Investigación de Materiales, Panamá, 0824, Panamá

ᵍInstitute of Nanotechnology (INT), Karlsruhe Institute of Technology (KIT), Kaiserstraße 12, D-76131 Karlsruhe, Germany

ʰKarlsruhe Nano Micro Facility (KNMFi), Karlsruhe Institute of Technology (KIT), Kaiserstraße 12, D-76131 Karlsruhe, Germany

ⁱCentre Européen de Sciences Quantiques (CESQ), Institut de Science et d'Ingénierie Supramoléculaires (ISIS), 8 allée Gaspard Monge, BP 70028, 67083 Strasbourg Cedex, France

†Electronic supplementary information (ESI) available: cif files, further synthetic details, structural and magnetic plots. CCDC 2354974. For ESI and crystallographic data in CIF or other electronic format see DOI: https://doi.org/10.1039/d4dt01588f

Ln = Tb(III) and Dy(III).[3] In lanthanide-based molecules, the anisotropic magnetic character is attributed to the intrinsic spin–orbit coupling of the first-order orbital angular momentum and the crystal field imposed by the ligand set giving rise to the single molecule magnet (SMM) behaviour.[3] In the case of lanthanide-based SMMs the anisotropy arises due to its intrinsic strong spin–orbit coupling (SOC) at single ion level,[4–6] while in 3d-based SMMs, the anisotropic character is attributed to the cooperative contribution of spin and local magnetic anisotropy leading to a large molecular spin ground state (S) with negative zero-field splitting (D).[7] A detailed understanding of the physical parameters playing a role in the anisotropic characteristics of lanthanide-based SMMs has led to energy barriers far larger than those observed in the 3d-based SMM analogues, ultimately realising blocking barriers above liquid nitrogen temperatures,[8,9] making these systems excellent candidates for high-density data storage devices. Furthermore, the comprehension and manipulation of the structural, electronic and nuclear characteristics of these systems, through a rational design, make these systems also candidates for quantum information processing schemes acting as qubits.[10–12] Today, SMMs have been proposed as qubits and qudits[10–15] – the quantum computer scaffolds –, quantum sensors,[16,17] quantum simulators[18–23] and quantum error correction protocols.[24–26] Notably, the execution of the quantum algorithm of Grover using a single molecule of TbPc₂ exemplifies the plausibility of SMMs being part of novel quantum technologies.[27]

To further the development of favourable SMM properties and finally implement lanthanide-based molecules in devices,

a detailed understanding of their magnetic properties continues to be a critical step.[28–31] A great deal of work has shed some light on the understanding of the magnetic behaviour of single lanthanide ion molecules,[32–38] denoting the importance of the role of magnetic interaction in SMMs. This understanding is required since polymetallic lanthanide clusters can show some unusual physical properties such as the observation of a toroidal magnetic[39–41] and strong magnetic exchange, causing an increment of the blocking temperatures.[9,35,42–44] Furthermore, by use of 3d ions in a $\{Cr_2Dy_2\}$ "butterfly" complex,[9,45–47] it has been shown that strong magnetic interaction can lead to hysteresis which is not observed when the exchange interactions are switched off using the diamagnetic 3d metal analogue. The operative anisotropic exchange in a $[Dy_4(O_2CNiPr_2)_{12}]$ has also proven important in obtaining a ferromagnetic and antiferromagnetic ground state, contingent upon the applied field direction.[48] In addition, coupling the electron spins in lanthanides has made it possible to indirectly couple the nuclear spins, which might be exploited as qudits.[49–51] Notably, recently it has been shown that a σ-bond between two lanthanide ions can lead to remarkably large hysteresis loops[9,47] even near the liquid nitrogen temperature region.[9]

In all cases above, magnetic interactions improve the magnetic characteristics of the SMMs. However, magnetic interactions between lanthanides in polymetallic systems can often likewise lead to faster relaxation rates, diminishing the SMM properties.[38,52–59] A common strategy to decrease such undesired effects is to dilute the SMM into an isostructural diamagnetic host. Experimentally the direct determination *via* electron paramagnetic resonance (EPR), in cohort with other techniques, unravelled the effect of exchange interactions operating between two distinct Dy(III) ions in an asymmetric dimer with the formula $[hqH_2][Dy_2(hq)_4(NO_3)_3]$ (hqH = 8-hydroxyquinoline).[38] In this system, the exchange interaction yields a well-separated manifold of four exchange states, which permit facile relaxation of the magnetisation at low temperatures, yielding no SMM behaviour in contrast to the diluted (*i.e.*, single ion) complex. Further studies on the analogous Ln(II) derivatives shed light on the coupling mechanism in such asymmetric systems.[34] Herein we report the exchange characteristic of a trinuclear dysprosium system. The 8-hydroxyquinoline ligand has been chosen due to its strong chelating effect.[60–63] A synthetic drawback of employing oxyquinolines is their tendency to form insoluble polymeric materials, making structural characterisation difficult. Usual routes therefore employ long high-temperature reactions to try and isolate the thermodynamic product.[60–62] In our approach, the asymmetric trimetallic dysprosium complex with formula $[Dy_3(hq)_7(NO_3)_2(OH_2)]$ was obtained with mild reaction conditions. Conventional SQUID studies show an out-of-phase component of the AC magnetic susceptibility, characteristic of SMMs. Furthermore, sub-Kelvin characterisation employing a μSQUID array shows open hysteresis loops confirming the SMM character. The angular-dependent loops reveal a distinct magnetic behaviour, implying the existence of spin canting in

the system, in agreement with CASSCF calculations. The SMM behaviour in the complex is a concerted behaviour of the three Dy(III) ions connected by an antiferromagnetic intramolecular interaction, as experimentally determined and verified through simulations.

Results and discussion

Synthesis and crystallography

The direct reaction of $Dy(NO_3)_3 \cdot nH_2O$ and 8-hydroxyquinoline in the presence of Et_3N in acetonitrile under reflux conditions yields a bright orange solution, which upon slow evaporation affords single crystals suitable for X-ray studies (see ESI† section 1.1). In contrast to other approaches where elevated temperatures are required,[60–62,64,65] herein a rather mild approach affords the complex. Note that a non-equimolar amount of Et_3N was required to obtain a clear solution. In contrast, an equimolar amount of Et_3N based on the 8-hydroxyquinoline ligand led to the immediate formation of an insoluble product, while the absence of the base resulted in the formation of a slurry. Based on these points, it can be noted that the presence of the Et_3N is key for the formation of the complex under milder conditions. The compound $[Dy_3(hq)_7(NO_3)_2(H_2O)]$ crystallises in the $P\bar{1}$ space group with one molecule residing in the asymmetric unit, while two and a half molecules complete the unit cell (Fig. 1A and Table S1†). Three Dy(III), seven 8-quinolinates (hq), two nitrate ions (NO_3) and one terminal water molecule complete the structure, while 2.5 molecules of solvents are found in the lattice, yielding a complex with the formula $[Dy_3(hq)_7(NO_3)_2(H_2O)] \cdot 2.5MeCN$ (Fig. 1B). The metal core resembles the previously reported $\{Dy_3\}$ with a "V-shaped"[60] motif and possess a Dy(1)⋯Dy(2)⋯Dy(3) angle of 149.78°. The Dy⋯Dy separations are 3.5592(6) Å and 3.5120(6) Å for Dy(1)⋯Dy(2) and Dy(2)⋯Dy(3), respectively. Three different coordination environments are observed for the dysprosium centres; Dy(1) and Dy(2) present a square antiprismatic geometry with a continuous shape measure (CShM)[66] of 1.364 and 1.129, respectively, whilst Dy(3) shows a spherical tricapped trigonal prismatic geometry (CShM of 2.232) (see Table S2 and Fig. S1†). The chelating ligands bind the three dysprosium centres with a mixture of μ–$1\kappa(N,O):2\kappa(O)$ bridging ligands. The coordination sphere of Dy(1) is filled by four hq groups and one terminal H_2O giving a N_3O_5 donor set, whilst six hq ligands give Dy(2) an N_2O_6 donor environment. Finally, Dy(3) is bridged by three hq and two chelating NO_3 anions leading to an N_2O_7 donor set. Both nitrate ions bind with the 1.110 coordination mode (see Harris notation).[67] The packed structure shows π–π interactions with the shortest distance between hq groups being 3.318 Å, with MeCN solvent molecules residing in pockets between the complexes. The shortest intermolecular Dy⋯Dy distance is 6.0421(6) Å.

Magnetic studies

The magnetic behaviour of $[Dy_3(hq)_7(NO_3)_2(H_2O)]$ was investigated on polycrystalline samples in the temperature range
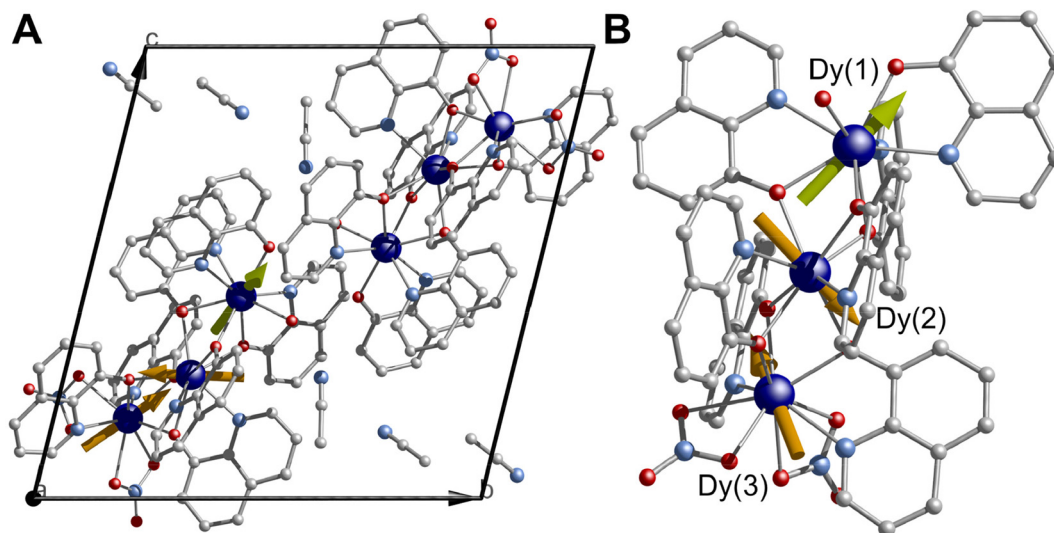
Fig. 1 Crystal structure of [**Dy₃(hq)₇(NO₃)₂(H₂O)**]·2.5MeCN. (A) Unit cell viewed along the crystallographic *a*-axis, showing the two symmetrically equivalent molecules of [**Dy₃(hq)₇(NO₃)₂(H₂O)**] filling the unit cell; (B) molecular structure of [**Dy₃(hq)₇(NO₃)₂(H₂O)**]. The arrows represent the orientation of the principal magnetic axes for Dy(1), Dy(2) and Dy(3) in the ground Kramers doublet from *ab initio* calculations shown as green arrows and orange arrows. Colour code: Dy, blue; N, light blue; O, red; C, grey. Hydrogen atoms were omitted for clarity.

2–300 K under an applied DC magnetic field (H_{DC}) of 1 kOe. The room temperature $\chi_M T$ value (being χ_M the molar magnetic susceptibility) for this system is found to be 42.2 cm³ K mol⁻¹, in good agreement with the $\chi_M T$ expected for the sum of three non-interacting Dy(III) ions (42.5 cm³ K mol⁻¹, with g_J = 4/3, J = 15/2). Upon cooling the $\chi_M T(T)$ faintly decreases down to about 50 K when it decreases faster reaching a value of 22.9 cm³ K mol⁻¹ at 2 K (Fig. 2A). The drop upon lowering the temperature observed can be attributed to a gradual depopulation of the crystal field split m$_J$ sublevels of the ground J multiplet, while magnetic interactions between the Dy(III) sites cannot be excluded.

The dynamic magnetic behaviour was likewise studied employing a SQUID magnetometer. In this case, AC susceptibility measurements were carried out between 2 and 10 K without an applied H_{DC} field. A clear temperature and frequency dependence of the in- ($\chi'_M(T;\nu)$) and out-of-phase ($\chi''_M(T;\nu)$) magnetic susceptibility profiles were observed. This behaviour can be directly ascribed to blockage to the relaxation of the magnetisation, a behaviour characteristic of SMMs. In the $\chi''_M(T)$ a maximum is observed at *ca.* 8 K at the highest frequency (1512 Hz) (Fig. 2C). At the lowest temperature, the maximum in the $\chi''_M(\nu)$ is centred at *ca.* 121 Hz and stays centred at this frequency up to *ca.* 5 K. The constant behaviour of the $\chi''_M(\nu)$ traces upon temperature increment, can be directly ascribed to the quantum tunnelling of the magnetisation (QTM) being operative. Above 5 K, the maximum in $\chi''_M(\nu)$ shifts swiftly towards higher frequencies up to 9.8 K where the maximum lies outside our experimental frequency window (Fig. 2D).

Simultaneous fitting the $\chi'_M(\nu)$ and $\chi''_M(\nu)$ to a generalised Debye model allows the extraction of the temperature-dependent relaxation times $\tau(T)$ of the system. A relatively uniform

distribution of relaxation times is obtained, with 0.18(1) < α < 0.19(1) [from lowest to highest temperature], where a value of 0 would indicate no distribution. The obtained $\tau(T)$ data can be fitted to a multi-relaxation process employing the following equation:

$$\tau^{-1} = \tau_0^{-1} \exp(-U_{eff}/k_B T) + CT^n + \tau_{QTM}^{-1} \qquad (1)$$

with the first term being the Orbach process, the second one being the Raman and the third one being the QTM process. The best-fit yields the following parameters: τ_0 = 2.2(7) × 10⁻⁷ s, U_{eff} = 61(2) K, C = 1.5(7) s⁻¹ K⁻ⁿ, n = 2.8(3) and QTM = 12.2 (5) ms (Fig. 2B). Note that the Raman n parameter is smaller than expected for Kramers ions, which could be a consequence of low vibrations phonon-mediated relaxation.[68–70] To account for this, the second term in (1) can be replaced by:

$$\tau_{Raman}^{vib} = \sum_{i=1}^{n} C_i \frac{\exp\left(\frac{\hbar\omega_i}{k_B T}\right)}{\left(\exp\left(\frac{\hbar\omega_i}{k_B T}\right) - 1\right)^2} \qquad (2)$$

where the ω_i are the Raman vibrational modes.[68] A good fit is obtained solely with the inclusion of a single vibrational mode, yielding U_{eff} = 34(1) K (24(1) cm⁻¹), τ_0 = 6(1) × 10⁻⁶ s, C_1 = 341(260) s⁻¹, ω_1 = 5(1) cm⁻¹, τ_{QTM} = 1.21(2) × 10⁻³ s (Fig. S4†), with the ω_i being low.[68,71,72]

Although the AC profiles indicate that [**Dy₃(hq)₇(NO₃)₂(H₂O)**] is an SMM, confirmation of the SMM character was sought through the μSQUID technique at sub-Kelvin temperatures. μSQUID measurements were carried out in the temperature range of 4.5 K down to 30 mK using a dilution fridge with applied fields of ±1 T. Single crystals of [**Dy₃(hq)₇(NO₃)₂(H₂O)**] were directly placed on top of the μSQUID arrays, while the
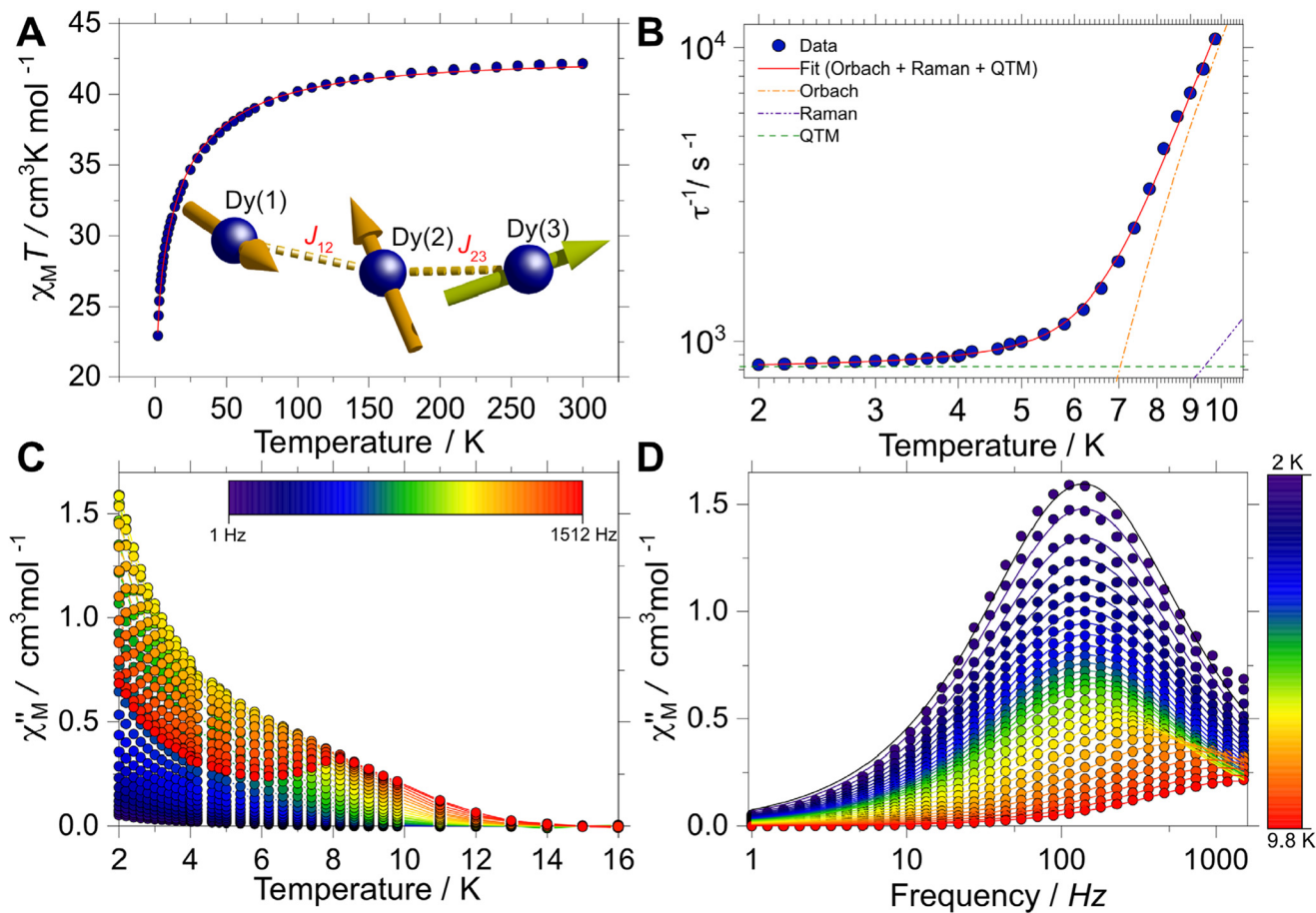
Fig. 2 (A) Experimental $\chi_M T(T)$ data for compound $[Dy_3(hq)_7(NO_3)_2(H_2O)]$; (B) $\tau(T)$ experimental data (blue symbols) obtained from the generalised Debye model and the fit to a model comprising the Raman, Orbach and QTM processes (solid line). The contribution of each process to the overall fit is shown as dotted lines; (C) temperature-dependent $\chi''_M(T)$ data (solid lines are guide for the eye) and (D) frequency-depended $\chi''_M(\nu)$ data (symbols) and generalised Debye analysis (solid lines).

field was applied along the magnetic anisotropy axis of the crystal employing the transverse field method.[73,74] Three types of studies were conducted: (i) temperature-dependent hysteresis loops from 30 mK up to 4.5 K at a fixed sweeping magnetic field rate of 64 mT s^{-1} (Fig. S5†); (ii) magnetic field sweep-rated dependent studies with sweeping rates of 1 to 128 mT s^{-1} at a fixed base temperature of 30 mK (Fig. 3A); and (iii) magnetic field angle dependence (with respect to the crystal orientation) at a fixed temperature of 30 mK and fixed scan rate (16 mT s^{-1}) (Fig. 3B).

Confirmation of the SMM behaviour was obtained in these studies. The temperature and sweep-rate dependent µSQUID loops show the characteristic behaviour expected for SMMs, i.e., the temperature-dependent loops show opening at the lowest temperature, which reduces upon warming due to enhanced thermal relaxation. While the sweep-dependent loops at 30 mK are wider at faster sweeping rates, indicating small QTM at the level-crossing, and hence slow thermal relaxation above 0.03 T. Moreover, the application of the magnetic field at different crystallographic angles (xy plane) shows a rather distinct magnetic behaviour. The latter behaviour can

be ascribed to spin canting[74] between the anisotropic magnetic axes present in $[Dy_3(hq)_7(NO_3)_2(H_2O)]$.

Electronic structure calculations

Ab initio calculations are an indispensable tool to elucidate the origin of the anisotropic character of lanthanide-containing systems due to the subtle and complex crystal field interactions.[75,76] Hence, the magnetic properties of $[Dy_3(hq)_7(NO_3)_2(H_2O)]$ were likewise investigated using CASSCF/RASSI/SINGLE_ANISO *ab initio* calculations. OpenMolcas was employed for the complete-active-space self-consistent field (CASSCF) calculations of the $[Dy_3(hq)_7(NO_3)_2(H_2O)]$ complex[77] (see ESI† section 1.4 for details). The crystal field splits the ground $^6H_{15/2}$ spin–orbit multiplet of Dy(III) into eight Kramer's doublets, *i.e.* $m_J = \pm 15/2, \pm 13/2, \ldots \pm 1/2$. The calculations show that solely one Dy(1) sites possess a strongly anisotropic character ($g_x \approx g_y = 0$ and $g_z = 20$ and the first excited state at 147 cm^{-1}), while for Dy(2) and Dy(3) the ions are far from pure $m_J = \pm 15/2$ states (*e.g.*, for Dy(1) $g_{x,y} \neq 0$ and $g_z < 20$ with the first excited state at 35 and 14 cm^{-1}, respectively). The first excited state for Dy(2) and Dy
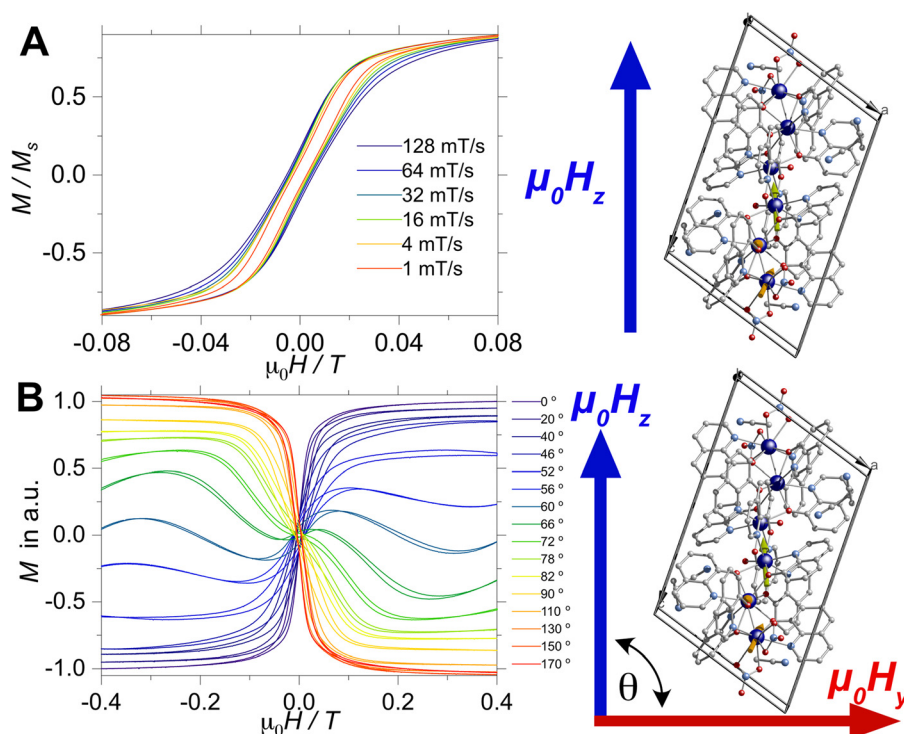
Fig. 3 (A) Magnetic field sweep-rated dependent studies with sweeping rates of 1 to 128 mT s^{-1} at a fixed temperature of 30 mK; (B) magnetic field angle (with respect to the crystal) dependence at a fixed temperature of 30 mK and fixed scan rate (16 mT s^{-1}). The top panels in A and B show the applied magnetic field during the measurements. While for A the magnetic field was kept static along the crystal, in B the magnetic field was varied at an angle θ. Note that the crystal orientation and the applied magnetic field might have an offset angle.

(3) is much more rhombic than the ground state and its main magnetic axis is not coincident with the ground state in all cases, while for Dy(1) the first excited state has a lower m_J component. These results suggest the environment for Dy(2) and Dy(3) is not ideal for stabilising the high angular momentum states of Dy(III), while Dy(1) should show an SMM character.

Up to this point, the discussion was based on the isolated Dy(III) ion, however, interactions between Dy(III) atoms can play a significant role in the relaxation dynamics. To evaluate the interaction operating between the Dy(III) ions, the Lines model[78] was employed to fit the magnetic susceptibilities of complexes **[Dy$_3$(hq)$_7$(NO$_3$)$_2$(H$_2$O)]**. The Lines model employs an isotropic exchange between the spin component of the angular momenta ($S = 5/2$ for Dy(III)) and the crystal field parameters obtained *via* the CASSCF calculations. The Hamiltonian has the form:

$$\mathcal{H}_{Dy}^i = \mathcal{H}_{lf}^i + g_J\mu_0\mu_B \sum_{i=1}^3 \hat{J}_{Dy(i)}H_z + J_{lines}^{12}\hat{S}_{Dy(1)}\hat{S}_{Dy(2)} + J_{lines}^{23}\hat{S}_{Dy(2)}\hat{S}_{Dy(3)}$$

(3)

where $\mathcal{H}_{lf}^i = \sum_{k=2,4,6,-k\leq q\leq k} B_k^q O_k^q$ is the ligand field Hamiltonian expressed in Steven's operator, O_k^q are the Stevens operator and B_k^q are the ligand field parameters obtained from CASSCF calculations. $\hat{J}_{Dy(i)}$ and $\hat{S}_{Dy(i)}$ are the spin–orbit and spin-only state

for Dy(III), respectively. Fitting[79] of $\chi_M T(T)$ employing the crystal field parameters as determined from CASSCF, yields a $J_{lines12} = -0.07(1)$ cm^{-1} and $J_{lines23} = -0.27(1)$ cm^{-1} with $R = 2.9$ (with $R = \sum_i^{points} [\chi_{exp} - \chi_{calc}]^2$) (see Fig. 2A). Attempts to fit the $\chi_M T(T)$ profile employing a single interaction produce a lower agreement and higher residual factors. Considering the Dy···Dy distances 3.5592(6) Å for Dy(1)···Dy(2) and 3.5120(6) for Dy(2)···Dy(3), and the strongest component of the dipolar interaction obtained for such distances (~-0.7 cm^{-1} projected on an $S = 5/2$ state), it is very probable that the interaction operating within **[Dy$_3$(hq)$_7$(NO$_3$)$_2$(H$_2$O)]** are of dipolar origin [see ESI† section 1.5].

Furthermore, the μSQUID loops show a clear angular dependence of the loops upon magnetic field application (see Fig. 3B). These observations are consistent with the anisotropy arrangement of the magnetic axes for the three Dy(III) systems, which depart from collinearity, in agreement with the CASSCF calculated spin projections. Given the polynuclear characteristics and the number of parameters characterising the system, a quantitative analysis of the angular μSQUID loops is not feasible. Nonetheless, a qualitative assessment of the spin canting effect in the μSQUID loops can be gained by simulating the Zeeman diagram at different field orientations. However, the large Hilbert space of the **[Dy$_3$(hq)$_7$(NO$_3$)$_2$(H$_2$O)]** and the number of parameters

involved, *e.g.*, ligand field parameters, *g*-values, Euler angles and exchange interaction, a *J* = 15/2 makes the rationalisation of the sub-Kelvin temperature data computationally expensive. To overcome this problem, the spin effective formalism (S_{eff} = 1/2) can be used. For simplicity, a single arbitrary interaction parameter and pure axial *g*-tensors were employed *i.e.*, one $g_{xx} = g_{yy} = 0$; $g_{zz} = 20$ (for m_J = 15/2) and two $g_{xx} = g_{yy} = 0$; $g_{zz} = 17$ (for m_J = 13/2) and the Euler angles [in *Z*–*Y*′–*Z*″ convention] for each Dy(III) ion obtained from the CASSCCF calculations. However, S_{eff} = 1/2, at first order, mixed strongly by transverse fields, prompting large tunnelling splitting, not representative of the system, hence, a fictitious *S* = 3/2 system with an arbitrarily large zero field splitting (*D*) parameter *D* = −100 cm^{-1} is found more suitable. The *g*-values were maintained isotropic ($g_{xx} = g_{yy} = g_{zz} = 20/3$ and $g_{xx} = g_{yy} = 0$; $g_{zz} = 17/3$), since the anisotropy is projected on the ZFS, while the anisotropy of the *D* term was rotated employing the Euler angles obtained from CASSCF.[71] The CASSCF results indicate that the single ion magnetic properties of **[Dy$_3$(hq)$_7$(NO$_3$)$_2$(H$_2$O)]** are dominated by the spin–orbit coupling and the interaction with the ligands, yielding a considerable separation between the ground and the first excited multiplet, as compared to the temperature bath. Therefore, we define the complex as three isolated Ising spins coupled through an effective interaction $J_{total}(\hat{S}_1 \cdot \hat{S}_2)$, where J_{total} is an effective coupling and $\hat{S}_1 \cdot \hat{S}_2$, are effective spin for each Dy(III). In the presence of an external mag-netic field applied along the easy axis, the Hamiltonian for **[Dy$_3$(hq)$_7$(NO$_3$)$_2$(H$_2$O)]** is:

$$\mathcal{H} = g_{eff}\mu_B\mu_0 H_z \sum_i^3 \hat{S}_i + J_{total}(\hat{S}_1 \cdot \hat{S}_2 + \hat{S}_2 \cdot \hat{S}_3) + \sum_i^3 \hat{S}_i \cdot D_i \cdot \hat{S}_i$$

(4)

The first term in (4) is the Zeeman term, the second the exchange interaction and the last the zero-field splitting. The non-colinear nature of the easy axes of the system is taken into consideration by employing the Euler rotations. The results show that the spin-canted arrangement of the Dy(III) ions in **[Dy$_3$(hq)$_7$(NO$_3$)$_2$(H$_2$O)]** and the interaction operating between the ions renders the lowest multiplet of the coupled system to be sensitive to the field direction. While applying the magnetic field along the easy axes of Dy(1) leads to a ferromagnetic ground state, applying the field perpendicular to the easy axis of Dy(1) renders a diamagnetic ground state. Bearing in mind that **[Dy$_3$(hq)$_7$(NO$_3$)$_2$(H$_2$O)]** the field is applied along an intermediate direction in the μSQUID arrays, it would cause different responses in the orientation-dependent loops as shown in Fig. 4.

As an overall result, although CASSCF predicts a highly pure m_J = 15/2 state for Dy(1), rather rhombic characteristics are found for Dy(2) and Dy(3) with large spin canting as determined by μSQUID results and CASSCF calculations.
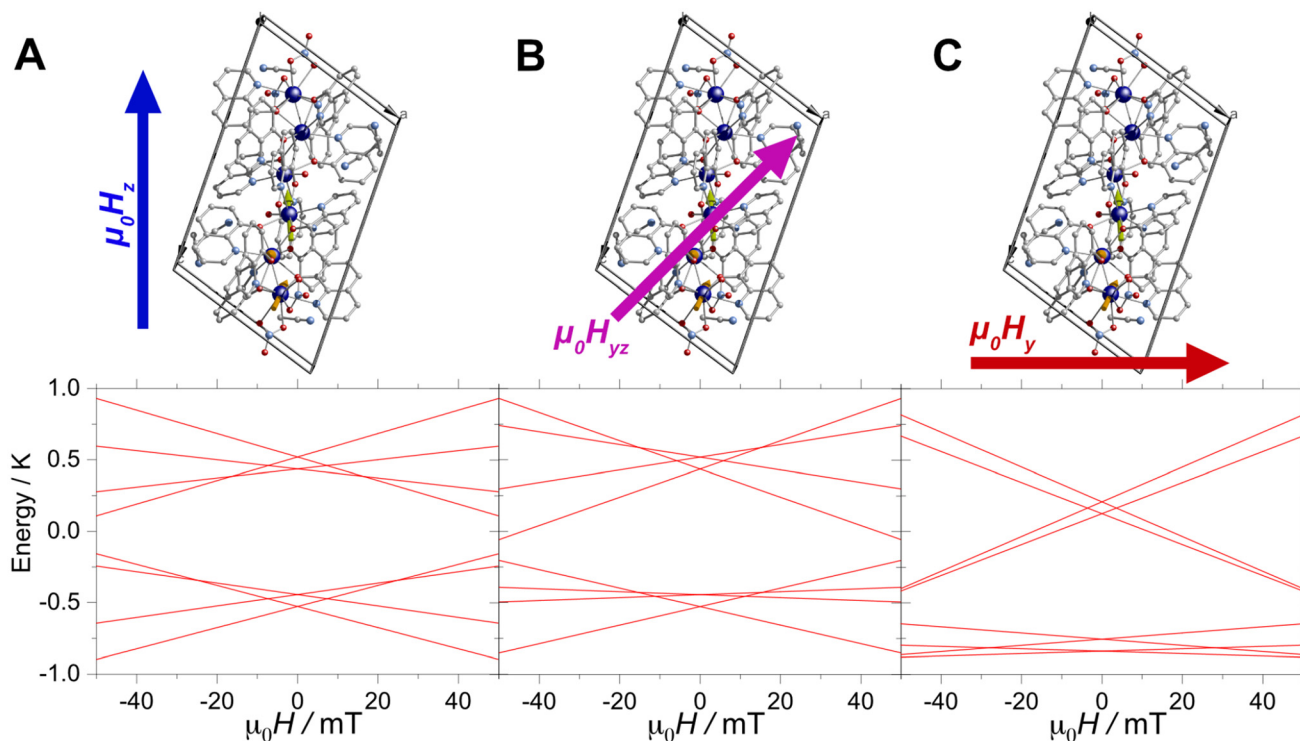
Fig. 4 Zeeman diagram for **[Dy$_3$(hq)$_7$(NO$_3$)$_2$(H$_2$O)]** with the applied field between the *a*−*c* crystallographic plane (A) the easy axes of Dy(1); (B) with the field 45° off the easy axes of Dy(1); and (C) with the field perpendicular to the easy axes of Dy(1). Application of the field along the easy axes of Dy(1) leads to a ferromagnetic ground state, while perpendicular to the easy axes the ground doublet is an antiferromagnetic state.

Conclusions

Herein we have described the synthesis of a heteroleptic dysprosium trimer with the formula $[Dy_3(hq)_7(NO_3)_2(H_2O)]$ under mild conditions. The compound shows a V-shaped geometry with a rather asymmetric arrangement. Magnetic studies reveal a clear SMM behaviour, further corroborated by µSQUID studies conducted at sub-Kelvin temperatures. Fitting the $\chi_M T(T)$ profile, employing the Lines model, shows that anti-ferromagnetic interactions couple the Dy(III) ions [$J_{lines12}$ = −0.07(1) cm^{-1} and $J_{lines23}$ = −0.27(1) cm^{-1}]. Comparison of the Lines interaction and the dipolar matrices operating between the systems suggest that the interactions in $[Dy_3(hq)_7(NO_3)_2(H_2O)]$ are of dipolar origin. µSQUID loops reveal open loops even at the lowest sweep rate and an angular-dependent character, while CASSCF calculations show that solely one of the dysprosium ion Dy(1) possesses SMM properties, with the remaining two having considerably rhombic characteristics. µSQUID and CASSCF results confirm the non-colinear spin arrangements of the systems, which along with the intramolecular antiferromagnetic interaction, are responsible for relaxation dynamics in $[Dy_3(hq)_7(NO_3)_2(H_2O)]$. When considering coupled systems, the electronic characteristics e.g., barriers, relaxation, QTM, differ from their single ion characteristics drastically. Often, for polynuclear complexes their electronic properties can be enhanced when all metallic ions are anisotropic with parallel or nearly parallel arrangements of spins,[36,80–82] while for non-colinear arrangements it has been usually observed that the properties are diminished.[38,58,83] In contrast, the interaction of the three Dy(III) ions in $[Dy_3(hq)_7(NO_3)_2(H_2O)]$ along with the canted spin arrangements, leads to a spin ground state with anisotropic characteristics and open loops and slow relaxation at zero field. This is a consequence of the nearly ferromagnetic ground state along the easy axes of $[Dy_3(hq)_7(NO_3)_2(H_2O)]$. Our results are in contrast with the behaviour of a $[hqH_2][Dy_2(hq)_4(NO_3)_3]$ complex, where the SMM character was quenched by the intramolecular interaction and the non-colinear spin arrangement with neighbouring non-SMM dysprosium site.[38] Herein we show the importance of the orientation of the easy axis and interactions in SMMs and the consequences, which might not completely quench the SMM character..

Author contributions

The idea was conceived by E. M.-P., C. M.-J., M. R. and W. W., J. J., E. M.-P. and C. M.-J. supervised the project. L. B., C. M.-J. and E. M.-P. carried out the AC and DC data collection, analysis and processing. S.P. and W. W. carried out the µSQUID data collection. D. F and O. F. carried out the crystallographic studies, data reduction and refinement. E. M.-P. and L. B. carried out the CASSCF calculations and interpretation. The data was analysed and interpreted by E. M.-P. with input from all co-authors. The manuscript was written by C.M.-J. and E.M.-P. with input from all co-authors.

Data availability

The data supporting this article has been included as part of the ESI.†

All the magnetic data was processed employing Origin Pro 2023. The Debye analysis and relaxation fits were also performed using Origin Pro 2023, while the $\chi_M T$ susceptibility data was fitted employing PHI (J. Comput. Chem., 2013, 34, 1164–1175). The Zeeman diagrams dependence of the µSQUID studies were obtained by employing Easyspin implemented in MATLAB (J. Magn. Reson. 2006, 178(1), 42–55).

Full crystallographic details can be found in CIF format: in the Cambridge Crystallographic Data Centre database (CCDC-2354974†).

Conflicts of interest

The authors declare no conflict of interest.

Acknowledgements

References

1   R. Sessoli, D. Gatteschi, H. L. Tsai, D. N. Hendrickson, A. R. Schake, S. Wang, J. B. Vincent, G. Christou and K. Folting, J. Am. Chem. Soc., 1993, 115, 1804–1816.
2   R. Sessoli, D. Gatteschi, A. Caneschi and M. A. Novak, Nature, 1993, 365, 141–143.
3   N. Ishikawa, M. Sugita, T. Ishikawa, S. Y. Koshihara and Y. Kaizu, J. Am. Chem. Soc., 2003, 125, 8694–8695.
4   L. Sorace, C. Benelli and D. Gatteschi, Chem. Soc. Rev., 2011, 40, 3092–3104.
5   W. T. Carnall, P. R. Fields and B. G. Wybourne, J. Chem. Phys., 1965, 42, 3797–3806.
6   D. N. Woodruff, R. E. P. Winpenny and R. A. Layfield, Chem. Rev., 2013, 113, 5110–5148.
7   D. Gatteschi, R. Sessoli and J. Villain, Molecular Nanomagnets, Oxford University Press, New York, 2007.
8   F. S. Guo, B. M. Day, Y. C. Chen, M. L. Tong, A. Mansikkamäki and R. A. Layfield, Science, 2018, 362, 1400–1403.
9   C. A. Gould, K. R. McClain, D. Reta, J. G. C. Kragskow, D. A. Marchiori, E. Lachman, E. Choi, J. G. Analytis, R. D. Britt, N. F. Chilton, B. G. Harvey and J. R. Long, Science, 2022, 375, 198–202.

10 E. Moreno-Pineda, C. Godfrin, F. Balestro, W. Wernsdorfer and M. Ruben, *Chem. Soc. Rev.*, 2018, **47**, 501–513.

11 A. Gaita-Ariño, F. Luis, S. Hill and E. Coronado, *Nat. Chem.*, 2019, **11**, 301–309.

12 F. Troiani and M. Affronte, *Chem. Soc. Rev.*, 2011, **40**, 3119–3129.

13 A. Chiesa, P. Santini, E. Garlatti, F. Luis and S. Carretta, *Rep. Prog. Phys.*, 2024, **87**.

14 M. Chizzini, L. Crippa, A. Chiesa, F. Tacchino, F. Petiziol, I. Tavernelli, P. Santini and S. Carretta, *Phys. Rev. Res.*, 2022, 1–15, 043135.

15 L. E. Nodaraki, A.-M. Ariciu, D. N. Huh, J. Liu, D. O. T. A. Martins, F. Ortu, R. E. P. Winpenny, N. F. Chilton, E. J. L. McInnes, D. P. Mills, W. J. Evans and F. Tuna, *J. Am. Chem. Soc.*, 2024, **146**, 15000–15009.

16 F. Troiani, A. Ghirri, M. G. A. Paris, C. Bonizzoni and M. Affronte, *J. Magn. Magn. Mater.*, 2019, **491**, 165534.

17 C. J. Yu, S. Von Kugelgen, D. W. Laorenza and D. E. Freedman, *ACS Cent. Sci.*, 2021, **7**, 712–723.

18 S. Chicco, G. Allodi, A. Chiesa, E. Garlatti, C. D. Buch, P. Santini, R. De Renzi, S. Piligkos and S. Carretta, *J. Am. Chem. Soc.*, 2024, **146**, 1053–1061.

19 A. Chiesa, P. Santini and S. Carretta, *Magnetochemistry*, 2016, **2**, 37.

20 A. Chiesa, G. F. S. Whitehead, S. Carretta, L. Carthy, G. A. Timco, S. J. Teat, G. Amoretti, E. Pavarini, R. E. P. Winpenny and P. Santini, *Sci. Rep.*, 2014, **4**, 7423.

21 M. Atzori, A. Chiesa, E. Morra, M. Chiesa, L. Sorace, S. Carretta, R. Sessoli, A. Chiesa, M. Chiesa, R. Sessoli, E. Morra, L. Sorace, M. Atzori, A. Chiesa, E. Morra, M. Chiesa, L. Sorace, S. Carretta and R. Sessoli, *Chem. Sci.*, 2018, **9**, 6183–6192.

22 P. Santini, S. Carretta, F. Troiani and G. Amoretti, *Phys. Rev. Lett.*, 2011, **107**, 230502.

23 A. Chiesa, S. Roca, S. Chicco, M. C. De Ory, A. Gómez-León, A. Gomez, D. Zueco, F. Luis and S. Carretta, *Phys. Rev. Appl.*, 2023, **19**, 35–37.

24 E. Macaluso, M. Rubín, D. Aguilà, A. Chiesa, L. A. Barrios, J. I. Martínez, P. J. Alonso, O. Roubeau, F. Luis, G. Aromí and S. Carretta, *Chem. Sci.*, 2020, **11**, 10337–10343.

25 A. Chiesa, E. Macaluso, F. Petiziol, S. Wimberger, P. Santini and S. Carretta, *J. Phys. Chem. Lett.*, 2020, **11**, 8610–8615.

26 A. Chiesa, F. Petiziol, E. Macaluso, S. Wimberger, P. Santini and S. Carretta, *AIP Adv.*, 2021, **11**, 025134.

27 C. Godfrin, A. Ferhat, R. Ballou, S. Klyatskaya, M. Ruben, W. Wernsdorfer and F. Balestro, *Phys. Rev. Lett.*, 2017, **119**, 187702.

28 A. Lunghi, *Sci. Adv.*, 2022, **8**, 7880.

29 S. Mondal and A. Lunghi, *J. Am. Chem. Soc.*, 2022, **144**, 22965–22975.

30 A. Chiesa, E. MacAluso, P. Santini, S. Carretta and E. Pavarini, *Phys. Rev. B*, 2019, **99**, 1–11.

31 E. Garlatti, S. Carretta, J. Schnack, G. Amoretti and P. Santini, *Appl. Phys. Lett.*, 2013, **103**, 222410.

32 P. E. Car, M. Perfetti, M. Mannini, A. Favre, A. Caneschi and R. Sessoli, *Chem. Commun.*, 2011, **47**, 3751–3753.

33 G. Cucinotta, M. Perfetti, J. Luzon, M. Etienne, P. E. Car, A. Caneschi, G. Calvez, K. Bernot and R. Sessoli, *Angew. Chem., Int. Ed.*, 2012, **51**, 1606–1610.

34 M. J. Giansiracusa, E. Moreno-Pineda, R. Hussain, R. Marx, M. Martínez Prada, P. Neugebauer, S. Al-Badran, D. Collison, F. Tuna, J. Van Slageren, S. Carretta, T. Guidi, E. J. L. McInnes, R. E. P. Winpenny and N. F. Chilton, *J. Am. Chem. Soc.*, 2018, **140**, 2504–2513.

35 C. Uhlmann, L. Münzfeld, A. Hauser, T. T. Ruan, S. Kumar Kuppusamy, C. Jin, M. Ruben, K. Fink, E. Moreno-Pineda and P. W. Roesky, *Angew. Chem., Int. Ed.*, 2024, **63**, e202401372.

36 M. G. Bernbeck, A. P. Orlova, J. D. Hilgar, M. Gembicky, M. Ozerov and J. D. Rinehart, *J. Am. Chem. Soc.*, 2024, **146**, 7243–7256.

37 W. Yang, G. Velkos, S. Sudarkova, B. Büchner, S. M. Avdoshenko, F. Liu, A. A. Popov and N. Chen, *Inorg. Chem. Front.*, 2022, **9**, 5805–5819.

38 E. Moreno-Pineda, N. F. Chilton, R. Marx, M. Dörfel, D. O. Sells, P. Neugebauer, S. Da Jiang, D. Collison, J. Van Slageren, E. J. L. McInnes and R. E. P. Winpenny, *Nat. Commun.*, 2014, **5**, 5243.

39 J. Tang, I. Hewitt, N. T. Madhu, G. Chastanet, W. Wernsdorfer, C. E. Anson, C. Benelli, R. Sessoli and A. K. Powell, *Angew. Chem., Int. Ed.*, 2006, **45**, 1729–1733.

40 J. M. Ashtree, I. Borilović, K. R. Vignesh, A. Swain, S. H. Hamilton, Y. L. Whyatt, S. L. Benjamin, W. Phonsri, C. M. Forsyth, W. Wernsdorfer, A. Soncini, G. Rajaraman, S. K. Langley and K. S. Murray, *Eur. J. Inorg. Chem.*, 2021, **2021**, 435–444.

41 H. L. Zhang, Y. Q. Zhai, L. Qin, L. Ungur, H. Nojiri and Y. Z. Zheng, *Matter*, 2020, **2**, 1481–1493.

42 J. D. Rinehart, M. Fang, W. J. Evans and J. R. Long, *Nat. Chem.*, 2011, **3**, 538–542.

43 J. D. Rinehart, M. Fang, W. J. Evans and J. R. Long, *J. Am. Chem. Soc.*, 2011, **133**, 14236–14239.

44 A. Hauser, L. Münzfeld, S. Schlittenhardt, C. Uhlmann, L. Leyen, E. Moreno-Pineda, M. Ruben and P. W. Roesky, *J. Am. Chem. Soc.*, 2024, **146**, 13760–13769.

45 S. K. Langley, D. P. Wielechowski, V. Vieru, N. F. Chilton, B. Moubaraki, B. F. Abrahams, L. F. Chibotaru and K. S. Murray, *Angew. Chem., Int. Ed.*, 2013, **52**, 12014–12019.

46 S. K. Langley, D. P. Wielechowski, V. Vieru, N. F. Chilton, B. Moubaraki, L. F. Chibotaru and K. S. Murray, *Chem. Sci.*, 2014, **5**, 3246–3256.

47 H. Kwon, K. R. McClain, J. G. C. Kragskow, J. K. Staab, M. Ozerov, K. R. Meihaus, B. G. Harvey, E. S. Choi, N. F. Chilton and J. R. Long, *J. Am. Chem. Soc.*, 2024, **146**(27), 18714–18721.

48 E. M. Pineda, Y. Lan, O. Fuhr, W. Wernsdorfer and M. Ruben, *Chem. Sci.*, 2017, **8**, 1178–1185.

49 E. Moreno-Pineda, S. Klyatskaya, P. Du, M. Damjanović, G. Taran, W. Wernsdorfer and M. Ruben, *Inorg. Chem.*, 2018, **57**, 9873–9879.

50 H. Biard, E. Moreno-Pineda, M. Ruben, E. Bonet, W. Wernsdorfer and F. Balestro, *Nat. Commun.*, 2021, **12**, 4443.

51 T.-T. Ruan, E. Moreno-Pineda, M. Schulze, S. Schlittenhardt, T. Brietzke, H.-J. Holdt, S. K. Kuppusamy, W. Wernsdorfer and M. Ruben, *Inorg. Chem.*, 2023, **62**, 15148–15156.

52 F. Habib and P. Lin, *J. Am. Chem. Soc.*, 2011, **133**, 8830–8833.

53 R. J. Blagg, L. Ungur, F. Tuna, J. Speak, P. Comar, D. Collison, W. Wernsdorfer, E. J. L. McInnes, L. F. Chibotaru and R. E. P. Winpenny, *Nat. Chem.*, 2013, **5**, 673–678.

54 R. J. Blagg, F. Tuna, E. J. L. McInnes and R. E. P. Winpenny, *Chem. Commun.*, 2011, **47**, 10587–10589.

55 R. J. Blagg, C. A. Muryn, E. J. L. McInnes, F. Tuna and R. E. P. Winpenny, *Angew. Chem., Int. Ed.*, 2011, **50**, 6530–6533.

56 R. J. Blagg, L. Ungur, F. Tuna, J. Speak, P. Comar, D. Collison, W. Wernsdorfer, E. J. L. McInnes, L. F. Chibotaru and R. E. P. Winpenny, *Nat. Chem.*, 2013, **5**, 673–678.

57 A. Bhanja, E. Moreno-Pineda, R. Herchel, W. Wernsdorfer and D. Ray, *Dalton Trans.*, 2020, **49**, 7968–7976.

58 Y. S. Meng, Y. Sen-Qiao, M. W. Yang, J. Xiong, T. Liu, Y. Q. Zhang, S. Da Jiang, B. W. Wang and S. Gao, *Inorg. Chem. Front.*, 2020, **7**, 447–454.

59 N. Lalioti, V. Nastopoulos, N. Panagiotou, A. Tasiopoulos, N. Ioannidis, J. Van Slageren, P. Zhang, G. Rajaraman, A. Swain and V. Tangoulis, *Dalton Trans.*, 2022, **51**, 1985–1994.

60 N. F. Chilton, G. B. Deacon, O. Gazukin, P. C. Junk, B. Kersting, S. K. Langley, B. Moubaraki, K. S. Murray, F. Schleife, M. Shome, D. R. Turner and J. A. Walker, *Inorg. Chem.*, 2014, **53**, 2528–2534.

61 G. B. Deacon, C. M. Forsyth, P. C. Junk and A. Urbatsch, *Eur. J. Inorg. Chem.*, 2010, **3**, 2787–2797.

62 G. B. Deacon, T. Dierkes, M. Hübner, P. C. Junk, Y. Lorenz and A. Urbatsch, *Eur. J. Inorg. Chem.*, 2011, 4338–4348.

63 F. Artizzu, P. Deplano, L. Marchiò, M. L. Mercuri, L. Pilia, A. Serpe, F. Quochi, R. Orrù, F. Cordella, F. Meinardi, R. Tubino, A. Mura and G. Bongiovanni, *Inorg. Chem.*, 2005, **44**, 840–842.

64 G. B. Deacon, P. C. Junk and S. G. Leary, *Z. Anorg. Allg. Chem.*, 2004, **630**, 1541–1543.

65 G. B. Deacon, P. C. Junk, S. G. Leary and A. Urbatsch, *Z. Anorg. Allg. Chem.*, 2012, **638**, 2001–2007.

66 S. Alvarez, P. Alemany, D. Casanova, J. Cirera, M. Llunell and D. Avnir, *Coord. Chem. Rev.*, 2005, **249**, 1693–1708.

67 R. A. Coxall, S. G. Harris, D. K. Henderson, S. Parsons, P. A. Tasker and R. E. P. Winpenny, *Dalton Trans.*, 2000, 2349–2356.

68 M. Briganti, F. Santanni, L. Tesi, F. Totti, R. Sessoli and A. Lunghi, *J. Am. Chem. Soc.*, 2021, **143**, 13633–13645.

69 L. Münzfeld, M. Dahlen, A. Hauser, N. Mahieu, S. K. Kuppusamy, J. Moutet, M. Tricoire, R. Köppe, L. La Droitte, O. Cador, B. Le Guennic, G. Nocton, E. Moreno-Pineda, M. Ruben, P. W. Roesky, E. Moreno-Pineda, M. Ruben and P. W. Roesky, *Angew. Chem.*, 2023, **135**, 2023.

70 C. A. P. Goodwin, D. Reta, F. Ortu, N. F. Chilton and D. P. Mills, *J. Am. Chem. Soc.*, 2017, **139**, 18714–18724.

71 J. Wang, J. J. Zakrzewski, M. Zychowicz, Y. Xin, H. Tokoro, S. Chorazy and S.-I. Ohkoshi, *Angew. Chem., Int. Ed.*, 2023, **62**, e202306372.

72 F. S. Santana, M. Perfetti, M. Briganti, F. Sacco, G. Poneti, E. Ravera, J. F. Soares and R. Sessoli, *Chem. Sci.*, 2022, **13**, 5860–5871.

73 W. Wernsdorfer, N. E. Chakov and G. Christou, *Phys. Rev. B: Condens. Matter Mater. Phys.*, 2004, **70**, 132413.

74 P. Subedi, A. D. Kent, B. Wen, M. P. Sarachik, Y. Yeshurun, A. J. Millis, S. Mukherjee and G. Christou, *Phys. Rev. B: Condens. Matter Mater. Phys.*, 2012, **85**, 134441.

75 L. F. Chibotaru and L. Ungur, *J. Chem. Phys.*, 2012, **137**, 064112.

76 L. Ungur and L. F. Chibotaru, *Chem. – Eur. J.*, 2017, **23**, 3708–3718.

77 I. Fdez Galván, M. Vacher, A. Alavi, C. Angeli, F. Aquilante, J. Autschbach, J. J. Bao, S. I. Bokarev, N. A. Bogdanov, R. K. Carlson, *et al.*, *J. Chem. Theory Comput.*, 2019, **15**, 5925–5964.

78 M. E. Lines, *J. Chem. Phys.*, 1971, **55**, 2977–2984.

79 N. F. Chilton, R. P. Anderson, L. D. Turner, A. Soncini and K. S. Murray, *J. Comput. Chem.*, 2013, **34**, 1164–1175.

80 T. Han, M. J. Giansiracusa, Z. H. Li, Y. S. Ding, N. F. Chilton, R. E. P. Winpenny and Y. Z. Zheng, *Chem. – Eur. J.*, 2020, **26**, 6773–6777.

81 J. Wang, Q. W. Li, S. G. Wu, Y. C. Chen, R. C. Wan, G. Z. Huang, Y. Liu, J. L. Liu, D. Reta, M. J. Giansiracusa, Z. X. Wang, N. F. Chilton and M. L. Tong, *Angew. Chem., Int. Ed.*, 2021, **60**, 5299–5306.

82 H. S. Wang, P. F. Zhou, J. Wang, Q. Q. Long, Z. Hu, Y. Chen, J. Li, Y. Song and Y. Q. Zhang, *Inorg. Chem.*, 2021, **60**, 18739–18752.

83 M. Li, H. Wu, Z. Xia, V. Montigaud, O. Cador, B. Le Guennic, H. Ke, W. Wang, G. Xie and S. Chen, *Chem. Commun.*, 2019, **55**, 14661–14664.